Effect of chain unsaturation on the structure and thermotropic properties of galactocerebrosides

R. A. Reed and G. G. Shipley
Biophysics Institute, Departments of Medicine and Biochemistry, Boston University School of Medicine, Housman Medical Research Center, Boston, Massachusetts 02118

ABSTRACT Differential scanning calorimetry (DSC) and x-ray diffraction have been used to study the effect of increasing chain-unsaturation on the structure and properties of the hydrated cerebrosides *N*-stearoyl, -oleoyl, and -linoleoyl galactosylsphingosine (NSGS, NOGS, and NLnGS, respectively). DSC of hydrated (70 wt% water) NSGS shows an endothermic transition at 85°C (ΔH = 18.0 kcal/mol NSGS) and a broad exothermic transition at 40–60°C, the latter being dependent upon the previous cooling rate. X-Ray diffraction patterns recorded at 21, 61, and 86°C provide evidence for interconversions between metastable and stable crystalline NSGS bilayer phases. The properties of the unsaturated-chain cerebrosides are more complex. Hydrated NOGS shows a single endothermic transition at 44.8°C (ΔH = 11.5 kcal/mol NOGS). However, incubation of NOGS at 49°C for 24 h results in a second transition at 55.5°C. By cycling NOGS between 0 and 49°C complete conversion into this higher melting phase (ΔH = 12.1 kcal/mol NOGS) is achieved. X-ray diffraction confirms a bilayer phase at all temperatures and delineates the conversions between a crystalline phase at 21°C (bilayer period d = 56.5Å), a second crystalline phase at 47°C (d = 69.9Å), and a liquid crystalline phase at 59°C (d = 52.0Å). The more unsaturated NLnGS shows two transitions, a sharp transition at 28°C (ΔH = 8.0 kcal/mol NLGS) and a broad, low-enthalpy transition at 42°C (ΔH = 0.4 kcal/mol NLGS). Again, incubation between the two transitions leads to a single transition at 44°C (ΔH = 9.3 kcal/mol NLGS). X-ray diffraction demonstrates conversions between two crystalline bilayer phases (d = 55.2Å and d = 68.4Å), and a liquid crystalline bilayer phase (d = 51.8Å). Thus, increased unsaturation in the amide-linked fatty acyl chain of cerebrosides results in decreased chain-melting temperatures (NSGS > NOGS > NLnGS) and has marked effects on their structural properties.

INTRODUCTION

The lipid bilayer compartment of cell membranes is composed of many different classes of lipids, mainly phospholipids (e.g., phosphatidylcholine [PC], phosphatidylethanolamine), glycolipids (e.g., glycosyl diglycerides), glycosphingolipids (e.g., cerebrosides, gangliosides), and cholesterol. Phospholipids are the most abundant lipid class in animals, with each subclass (e.g., PC) containing variations in both chain-length and unsaturation of the glycerol-linked fatty acids. Many studies have focused on the chemical and physical properties of phospholipids. In contrast, glycosphingolipids have received much less attention compared to the glycerol-based phospholipids.

Cerebrosides, specifically galactocerebrosides are found in relatively large amounts in the central and peripheral nerve myelin (Linington and Rumsby, 1978; Rumsby, 1978), although their exact structural/functional role is not known. The structure and properties of cerebrosides have been studied by spectroscopic (Bunow and Levin, 1980; Skarjune and Oldfield, 1979, 1982; Huang et al., 1980; Lee et al., 1986), calorimetric (Clowes et al., 1971; Bunow, 1979; Freire et al., 1980; Linington and Rumsby, 1981; Curatolo, 1982, Curatolo and Jungalwala, 1985; Ruocco et al., 1981; Reed and Shipley, 1987), surface balance (Maggio et al., 1978a, b, 1981), and x-ray diffraction (Reiss-Husson, 1967; Abrahamsson et al., 1972, Fernandez-Bermudez et al., 1977; Hosemann et al., 1979; Ruocco et al., 1981; Reed and Shipley, 1987) methods. X-ray crystallography of synthetic cerebrosides demonstrate that the cerebroside molecules pack in a bilayer arrangement, with the galactosyl groups aligned almost parallel to the membrane interface (Pascher and Sundell, 1977). An extensive hydrogen bonding network, involving both inter- and intramolecular bonds, is formed through lateral interactions involving the galactose and sphingosine in the interfacial region.

The availability of homogeneously *N*-acylated cerebrosides has led to a greater understanding of the effect of hydrocarbon chain length on the physical properties of cerebrosides in bilayers. Ruocco et al. (1981) studied the properties of synthetic *N*-palmitoyl galactosylsphingosine (NPGS) by polarizing light microscopy, scanning calorimetry, and x-ray diffraction. Hydrated NPGS exhibited complex polymorphic behavior with interconversions between metastable and stable bilayer structures and gave a high-temperature (82°C), high-enthalpy (17.5 kcal/mol) bilayer crystal to liquid crystal transition. Similar, but not identical, observations were made for the

0006-3495/89/02/281/12 $2.00

corresponding glucosyl cerebroside (Freire et al., 1980). Using x-ray diffraction, Ruocco et al. (1981) demonstrated that the metastable form of NPGS was identical to an anhydrous crystal form and that the conversion to the stable form involved hydration of NPGS. Studies by Reed and Shipley (1987) utilizing hydrated *N*-lignoceroyl galactosylsphingosine (NLGS) indicated different polymorphic behavior compared with NPGS, and owing to kinetic problems, the exact nature of the metastability in NLGS could not be determined. However, it was apparent that the length of the amide-linked hydrocarbon chain in galactocerebrosides significantly altered the thermotropic and kinetic properties of the metastable phase. Studies differentiating between galactosyl cerebrosides containing hydroxylated and nonhydroxylated, amide-linked fatty acids (HFA-CER and NFA-CER) were carried out by Curatolo and Jungalwala (1985). Using calorimetry, HFA-CER were found to undergo crystal to liquid crystal transitions 10–20°C lower than the NFA-CER. HFA-CER also form metastable structures, however the presence of the 2-hydroxyl group resulted in a significant kinetic barrier to conversion to the stable form. Thus, chain-hydroxylation also influences cerebroside behavior.

The study of model membrane systems, where the chemical structure of a particular lipid (e.g., polar headgroup, chain linkage, chain length, and chain unsaturation) can be systematically changed, has increased our understanding of the function of these lipids in real membranes. Investigations concerning the effects of chain unsaturation on the properties of lipids in membranes have focused primarily on phospholipids and glycolipids, and not glycosphingolipids.

In phospholipid systems the fluorescent probe diphenylhexatriene (DPH) was employed to study the order and rate of motion of the fatty acyl chains of phosphatidylcholines (Stubbs et al., 1981). Upon introduction of a single *cis* double bond into saturated hydrocarbon chains, the order parameter decreased and the rate of motion increased, indicating that the hydrocarbon portion of the bilayer was less ordered. However, further increases in unsaturation had relatively little effect on these parameters, suggesting that the first double bond had the most significant structural effect. Coolbear et al. (1983), utilizing 18-carbon chain (C-18) phosphatidylcholines, demonstrated that the presence of the first *cis* double bond in the fatty acid (18:1, Δ9) at the sn-2 position, decreased the bilayer chain-melting temperature by about 50°C. A second double bond in the fatty acid (18:2, Δ9, 12) further reduced the chain-melting temperature by 12°C, and a third double bond (18:3, Δ9, 12, 15) actually began to increase the bilayer chain-melting transition (Coolbear et al., 1983). These studies indicated that as phosphatidylcholines become more unsaturated, the critical bilayer perturbation appears to be the addition of the first *cis* double bond.

In plants, glycolipids are the predominant lipid species, and in chloroplast membranes the major constituent is galactosyldiglyceride. Initial studies used x-ray diffraction to investigate the properties of monogalactosyldiglyceride (MGDG) and digalactosyldiglycerides (DGDG) and demonstrated that hydrated MGDG formed an inverted hexagonal phase (H_{II}) while DGDG remained in a lamellar bilayer phase (Shipley et al., 1973). Recently, the use of hydrogenation to obtain partially or fully saturated MGDGs has shown that only highly unsaturated MGDG forms hexagonal structures, while the less unsaturated MGDG and DGDG formed lamellar structures (Sen et al., 1981; Gounaris et al., 1983; Mannock et al., 1985; Mansourian and Quinn, 1986). Thus, for galactolipids, depending on the size of the headgroup, the degree of unsaturation within the hydrocarbon region can affect the type of membrane structure formed.

In contrast to phospholipids and glycolipids, little is known about the effect of hydrocarbon chain unsaturation on the properties of glycosphingolipids. We describe here a systematic study of the effect of unsaturation on C-18 chain galactocerebrosides using x-ray diffraction and differential scanning calorimetry (DSC).

MATERIALS AND METHODS

Samples

NSGS, NOGS, and *N*-linoleoyl galactosylsphingosine (NLnGS) were synthesized using pig brain cerebroside according to methods described by Skarjune and Oldfield (1979, 1982), based on the original isolation, deacylation and reacylation procedures of Radin (1972, 1974, 1976). The reacylated cerebrosides are estimated to contain approximately 5% of the dihydrosphingosine derivative. By thin-layer chromatography (TLC), NOGS and NLnGS gave a single spot in the solvent system chloroform/methanol/water (65:25:4, vol/vol) and were used without further purification. Impurities found in NSLS by TLC were removed using an Iatrobead column (catalogue No. 8060, Iatron Laboratories, Inc., Tokyo, Japan). Pure NSGS was recovered with a stepwise gradient of chloroform/methanol of increasing polarity.

Differential scanning calorimetry

Hydrated multilamellar samples were prepared by weighing NSGS, NOGS, and NLnGS separately into stainless-steel pans and adding double-distilled water to make 70 wt% water dispersions. The pans were hermetically sealed and each sample was cycled between temperatures above and below its transition temperatures to ensure equilibration (for details of additional equilibration protocols, see Results). Heating and cooling scans were performed on a Perkin-Elmer Corp. (Norwalk, CT) DSC-2C with heating and cooling rates ranging from 1.25°C/min to 40°C/min. Transition temperatures and enthalpies were determined using the DSC-2C microprocessor utilizing the TADS data analysis program. Overlapping DSC transitions observed on cooling were deconvoluted assuming symmetric peak shapes to give the enthalpies of the two transitions. Gallium was used as a standard. In experiments where

long-term incubation protocols were employed, the sample integrity was periodically checked by TLC.

X-Ray diffraction

Hydrated multilamellar x-ray samples were prepared by weighing NSGS, NOGS, and NLnGS separately into thin-walled (internal diameter = 1 mm) glass capillaries (Charles Supper Co., Natick, MA). Distilled water was added to make a 70 wt% water dispersion, followed by centrifugation to pack the dispersion at the bottom of the capillary. The capillaries were then flame-sealed, and the samples were centrifuged approximately 10 times through the capillary at a temperature above their transition temperature (see Results). The x-ray diffraction experiments were performed with nickel-filtered CuK_α x-radiation (λ = 1.5418Å) from an Elliot GX-6 rotating anode x-ray generator (Elliot Automation, Borehamwood, U.K.), focused by either a toroidal mirror or Franks mirror optical camera. The samples were kept at constant temperature by a circulating ethylene glycol/water bath with the temperature being monitored by a thermocouple adjacent to the sample. The diffraction patterns were recorded on Kodak No-screen x-ray film.

RESULTS

NSGS

The calorimetric behavior of hydrated (70 wt% H_2O) NSGS (18:0) is summarized in Fig. 1. Upon heating at 5°C/min (Fig. 1 *A*), equilibrated NSGS shows two transitions: a complex, broad exothermic transition from 40°C to 60°C (transition enthalpy $\Delta H = -1.7$ kcal/mol NSGS), and a high-temperature, high-enthalpy endothermic transition (T_m) at 85°C (ΔH = 18.0 kcal/mol NSGS). Fig. 1 *B* shows the behavior of NSGS on cooling at 5°C/min. Two transitions are observed, a sharp exotherm centered at 60°C and a broader exotherm at ~50°C with a combined enthalpy of −13.7 kcal/mol NSGS. Immediate reheating shows identical behavior to that shown in Fig. 1 *A*. In order to assess the reversibility of the broad exotherm observed on heating, NSGS was heated to 67°C (see Fig. 1 *C*, and immediately cooled (Fig. 1 *D*). Upon cooling no exothermic transitions are observed in the temperature range from 67°C to 5°C. Upon reheating (Fig. 1 *E*), no exotherm is seen in the temperature range 5–80°C, only the high-temperature, high-enthalpy endothermic transition (same T_m and ΔH as in Fig. 1 *A*). Thus, the broad exotherm observed on heating is irreversible. If the sample is now cooled from above the 85°C endotherm, the two exothermic transitions are observed (see Fig. 1 *F*, cf. Fig. 1 *B*). The subsequent heating scan shown in Fig. 1 *G* is identical to that shown in Fig. 1 *A*. Thus, the calorimetric data presented in Fig. 1 indicate that the exothermic behavior observed on heating hydrated NSGS (after cooling from $T > T_m$) represents the conversion (40–60°C) from a metastable low temperature form of NSGS to a thermodynamically stable form. This form is stable over the temperature range of 5–85°C, and is the form which undergoes the high-temperature

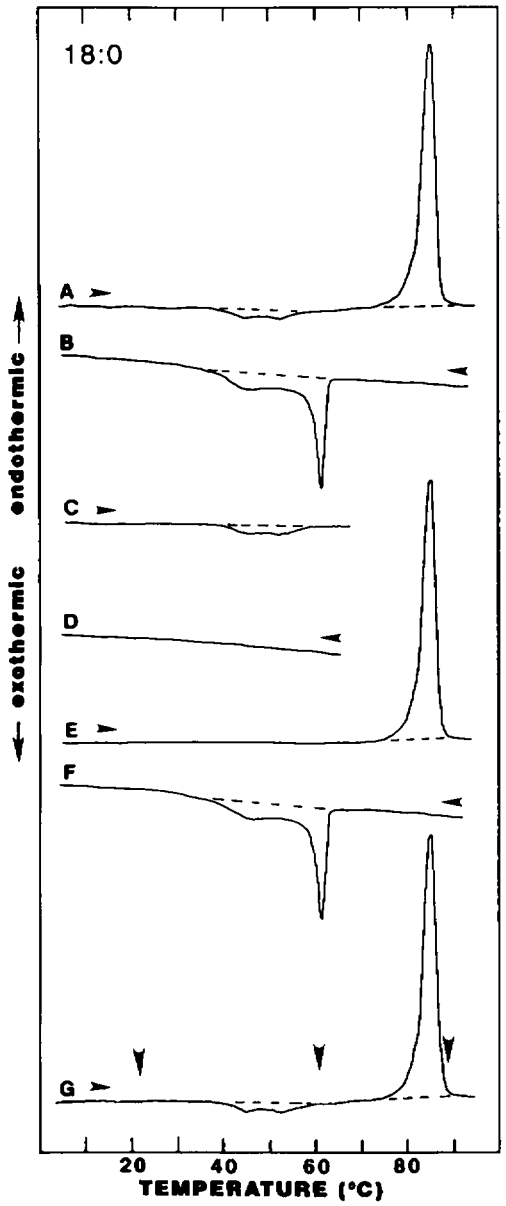

FIGURE 1 DSC scans of hydrated (70 wt% H_2O) NSGS recorded at heating and cooling rates of 5°C/min. (*A*) Heating scan; (*B*) cooling scan; (*C*) heating scan to 67°C; (*D*) subsequent cooling scan; (*E*) heating scan; (*F*) subsequent cooling scan; (*G*) heating scan. (*Horizontal arrows*) Direction of heating/cooling scans. (*Vertical arrows*) Temperatures at which x-ray diffraction patterns were recorded.

(85°C), high-enthalpy (ΔH = 18.0 kcal/mol NSGS) endothermic transition. All other phases below 85°C are metastable with respect to it. Only on cooling hydrated NSGS from the phase present at $T > 85$°C are the two exothermic transitions observed (60 and 50°C) resulting in the formation of the low-temperature NSGS phases (see below).

To investigate further the irreversible exothermic transition observed on heating NSGS and its relationship to the two exotherms seen on cooling, a series of cooling rate studies were performed. Fig. 2 *A* shows cooling curves at rates decreasing from 40°C to 1.25°C/min. At the fastest cooling rate, 40°C/min (Fig. 2 *A*, curve *a*), a single exothermic transition is observed at 50°C (exotherm I, see Fig. 2 *B*[*inset*]). With decreasing cooling rate in the range from 40°C to 1.25°C/min, the second exotherm (II, see Fig. 2 *B*[*inset*]) is observed and it occurs at progressively higher temperatures (25–58°C) and with progressively higher enthalpy ($\Delta H = -1.3$ to -11.2 kcal/mol NSGS) (see Fig. 2 *A*, curves *a–f*). The higher-temperature exotherm (*I*) is much less dependent on cooling rate, increasing in temperature from 50°C to 61°C, and in enthalpy from -6.1 to -7.2 kcal/mol NSGS. When NSGS is reheated at 5°C/min after the 40°C/min cooling scan, the enthalpy associated with the exothermic transition centered at ~50°C has increased to 6.0 kcal/mol NSGS (data not shown). However, with progressively slower prior cooling rates, the enthalpy associated with this transition decreases, until finally at a cooling rate of 2.5°C/min it reaches zero (data not shown). Fig. 2 *B* is a plot of the change in enthalpy of exotherms I and II observed on cooling, their combined enthalpy, and the broad exotherm III (*inset*) seen on reheating as a function of cooling rate. Clearly there is an inverse relationship between the enthalpy of exotherm II observed on cooling, and that of exotherm III observed on reheating. In contrast, exotherm I is essentially independent of cooling rate (see Fig. 2 *B*). Also represented in Fig. 2 *B* is a plot of the combined enthalpy of the two exotherms observed on cooling as a function of cooling rate (IV). At the slowest cooling rate used, 1.25°C/min, the sum of the enthalpy of the two exothermic transitions ($\Delta H = -18.3$ kcal/mol NSGS) is essentially identical to the enthalpy of the high-temperature, high-enthalpy endotherm observed on heating ($\Delta H = 18.0$ kcal/mol NSGS). Thus, it appears that the higher-temperature, cooling rate "independent" exotherm (I) observed on cooling represents the conversion of the NSGS sample to a metastable phase, whereas the cooling rate-dependent exotherms (II [cooling] and III [heating]) are associated with the formation of the stable phase of NSGS.

To elucidate the structural changes of hydrated NSGS, x-ray diffraction patterns were recorded at different temperatures following different equilibration conditions. The vertical arrows in Fig. 1 *G* correspond to temperatures at which the x-ray diffraction patterns shown in Fig. 3 were recorded. Fig. 3 *A* shows a diffraction pattern of hydrated (70 wt% water) NSGS recorded at 21°C after rapid cooling from 88°C; thus, it represents NSGS primarily in its metastable form (see calorimetry results, above). A series of lamellar reflections ($h = 1$–8) are

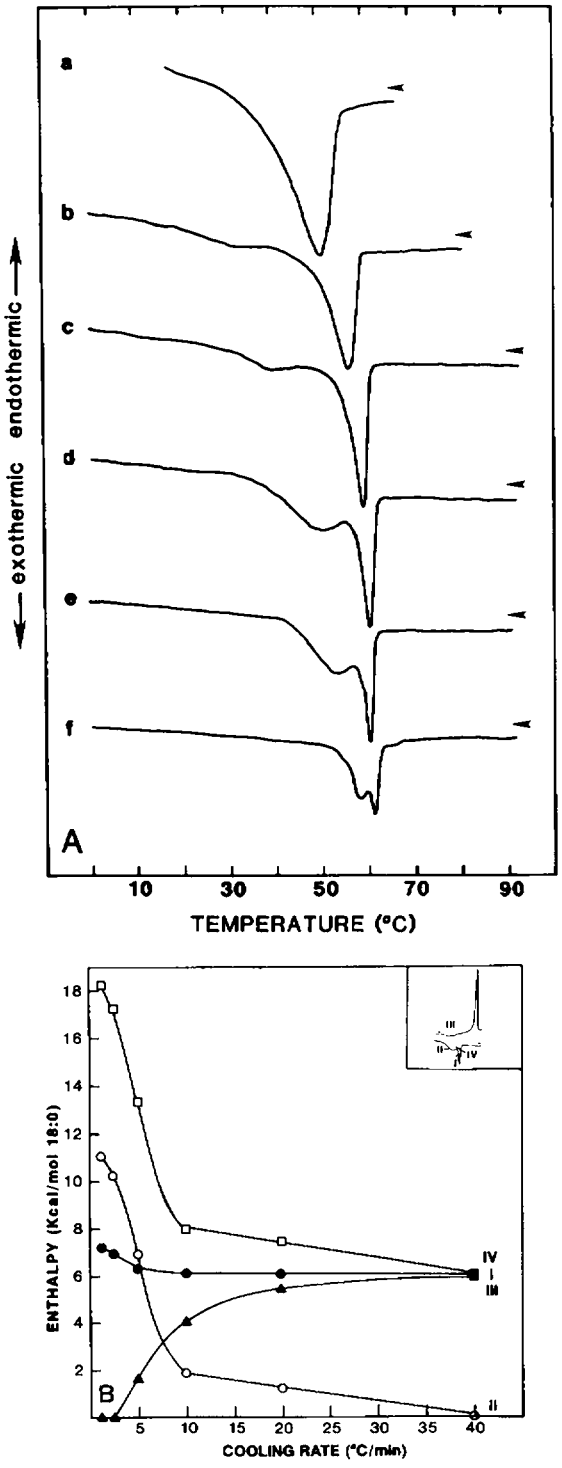

FIGURE 2 (*A*) DSC cooling scans of hydrated (70 wt% H_2O) NSGS recorded at (*a*) 40°C, (*b*) 20°C, (*c*) 10°C, (*d*) 5°C, (*e*) 2.5°C and (*f*) 1.25°C/min. (*B*) Transition enthalpies of different transitions observed on cooling (*inset*) as a function of cooling rate: (●) exotherm I; (○) exotherm II; (□) combined enthalpy (I and II), IV. In addition, the enthalpy associated with the exothermic transition observed on heating (5°C/min) immediately following cooling at different rates (▲, III).

observed corresponding to a bilayer periodicity, $d = 59.6$Å. Several reflections are observed in the wide-angle region, with the two strongest reflections appearing at 1/4.4 and 1/3.9Å^{-1} (*arrows*). Additional weaker reflections are observed at 1/5.9, 1/5.0, and 1/4.2Å^{-1}. Thus, under these conditions a complex wide-angle diffraction pattern is observed. The sample was then heated to 61°C corresponding to a temperature above the broad exotherm observed on heating (see *arrow*, Fig. 1 *G*), and the diffraction pattern was recorded (Fig. 3 *B*). The pattern shows minor changes in the position and intensities of the low-angle reflections $h = 1$–8, with $d = 58.4$Å. However, the wide-angle region shows some significant changes in intensity and position, notably the reflection at 1/4.2Å^{-1} (*arrow*) becoming the strongest and the absence of the reflection at 1/5.9Å^{-1}. Also, several additional weaker reflections are observed: 1/4.8, 1/4.5, 1/4.0, and 1/3.9Å^{-1}. Further heating to 86°C (above the high-temperature, high-enthalpy transition) yields a diffraction pattern characteristic of liquid-crystalline L_α bilayers (Fig. 3 *C*). The low-angle region contains four reflections ($h = 1$–4) corresponding to a bilayer period, $d = 53.7$Å. A single, diffuse reflection in the wide-angle region at 1/4.6Å^{-1} (*arrow*) is characteristic of melted hydrocarbon chains.

To identify the structural differences between the stable and metastable phases, a comparison was made between the metastable phase of NSGS and anhydrous NSGS. Fig. 4 *A* shows the diffraction pattern of hydrated NSGS rapidly cooled from the L_α phase (88°C) to 21°C. This "quenching" protocol was designed to favor the formation of the metastable phase at low temperatures. Fig 4 *B* is a diffraction pattern of anhydrous NSGS recorded at 22°C. The bilayer period for the anhydrous NSGS is 61Å (the odd order reflections are weak or absent), with two reflections in the wide angle region: a sharp, intense reflection at 1/4.5Å^{-1} (*arrow*) and a weaker, diffuse reflection at 1/3.9Å^{-1} (*arrow*). The diffraction pattern of the quenched, "metastable" form has a bilayer period of 60Å, similar to that of the anhydrous form (61Å) but the bilayer structure is apparently different (see differences in the intensity distribution); the strongest similarity is the presence of the two wide-angle reflections at ~1/4.5Å^{-1} (strong and sharp) and 1/3.9Å^{-1} (diffuse) (arrowed reflections in Fig. 4, *A* and *B*). Although it appears that the metastable form of NSGS exhibits some features of the anhydrous form, the analysis is further complicated by the presence of some of the stable phase even in this quenched sample (Fig. 4 *A*).

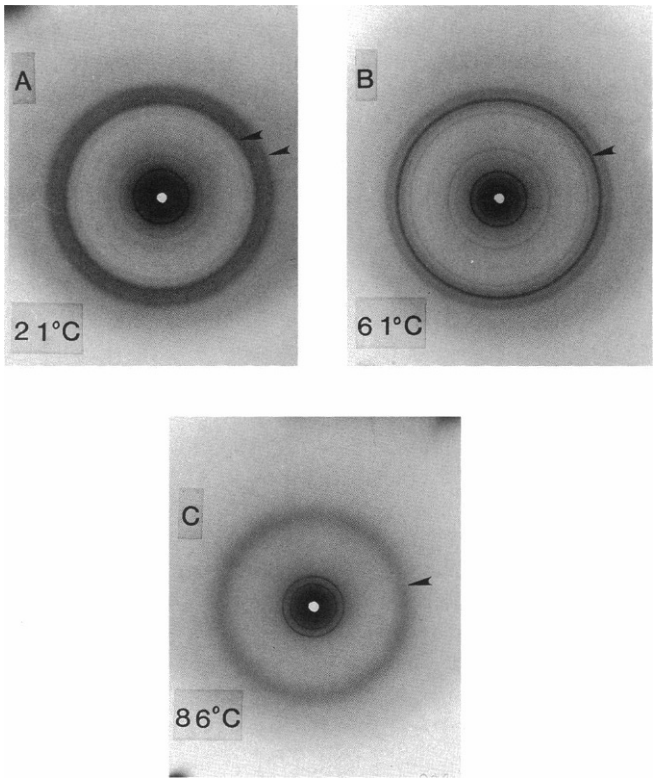

FIGURE 3 X-ray diffraction patterns of hydrated NSGS at (*A*) 21°C, (*B*) 61°C, and (*C*) 86°C.

NOGS

The calorimetric behavior of hydrated (70 wt% H_2O) NOGS (18:1) is summarized in Fig. 5. When equilibrated NOGS is heated at 5°C/min a single endothermic transition is observed (Fig. 5 *A*) centered at 44.8°C ($\Delta H = 11.5$ kcal/mol NOGS) suggestive of a chain-melting transition. Immediate cooling at 5°C/min (see Fig. 5 *B*) yields a sharp, exothermic transition at 22°C ($\Delta H = -11.5$ kcal/mol NOGS). However, x-ray diffraction patterns recorded at 47°C, a temperature just above the 44.8°C

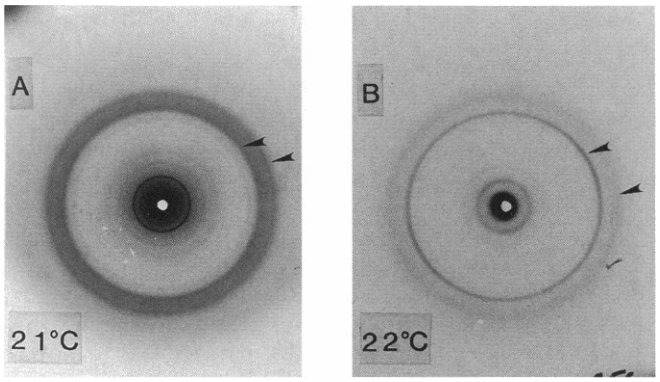

FIGURE 4 X-ray diffraction patterns of (*A*) hydrated NSGS at 21°C after cooling from 88°C, and (*B*) anhydrous NSGS.

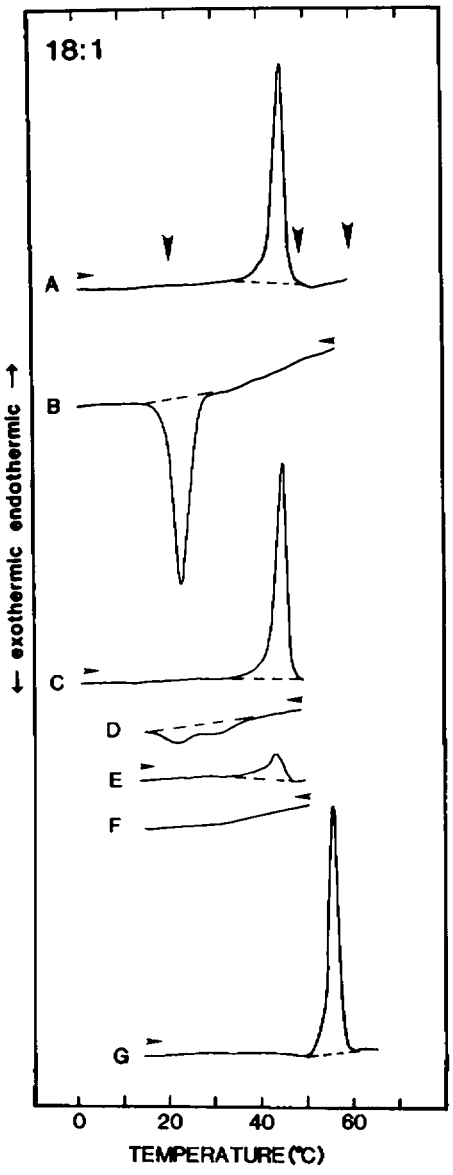

FIGURE 5 DSC scans of hydrated (70 wt % H_2O) NOGS recorded at heating and cooling rates of 5°C/min. (*A*) Heating scan; (*B*) cooling scan; (*C*) heating scan to 49°C; (*D*) subsequent cooling scan after incubation at 49°C for 24 h; (*E*) immediate heating scan to 49°C; (*F*) subsequent cooling scan after incubation at 49°C for 70 min; (*G*) heating scan. (*Horizontal arrows*) Direction of heating/cooling scans. (*Vertical arrows*) Temperatures at which x-ray diffraction patterns were recorded.

endotherm did not reveal a melted bilayer phase (see Fig. 6 *B*). This prompted the incubation experiments presented in Fig. 5, *C–G*. If hydrated NOGS is heated through the first endotherm to 49°C and incubated for 24 h (Fig. 5 *C*), the subsequent cooling curve (Fig. 5 *D*) reveals two broad transitions at 22°C and 29°C, and a decrease in the total enthalpy from −11.5 to −0.5 kcal/mol NOGS (cf. Fig. 5 *B*). If NOGS is again heated to 49°C (Fig. 5 *E*), the enthalpy associated with the 44.8°C transition is reduced from 11.5 to 1.8 kcal/mol NOGS. After a second incubation at 49°C, this time for only 70 min, the subsequent cooling run (Fig. 5 *F*) shows no transitions in the temperature range from 49°C to 15°C. Fig. 5 *G* shows the heating scan of NOGS immediately after the incubation protocol described above. No endotherm is observed at ~45°C, however a new transition appears at 55.5°C with an enthalpy of 12.1 kcal/mol NOGS indicating the formation of a second, higher melting phase. Interestingly, a minimum of two incubations is necessary to convert the form giving the 44.8°C endotherm into the higher melting form; a single incubation of up to several days at 49°C is not sufficient. Upon cooling and reheating NOGS from above the 55°C endotherm, the same behavior as in Fig. 5, *B* and *A*, is observed, i.e., re-formation of the original low temperature phase (T_m = 44.8°C).

The thermotropic behavior of hydrated NOGS indicates the existence of two forms. One form (form I) appears to be stable over the temperature range of 0–44°C, and undergoes endothermic chain melting at 44.8°C. This form is generated upon cooling if the sample is not incubated at $45 < T < 55$°C (see Fig. 5, *A–C*). However if NOGS is incubated at $45 < T < 55$°C, then a time-dependent transformation results in a higher-melting form (T_m = 55.5°C; form II). In principle, this higher-melting form should be the most stable form with all other low temperature phases (including form I) being metastable with respect to it.

The vertical arrows in Fig. 5 *A* corresponds to the temperatures at which the x-ray diffraction patterns shown in Fig. 6 were recorded. The diffraction pattern shown in Fig. 6 *A* is of the NOGS (form I) at 21°C. The low-angle region shows lamellar reflections (h = 1–9), bilayer periodicity d = 56.5Å. The wide-angle region shows five strong reflections at 1/5.6 (sharp), 1/5.1 (sharp), 1/4.7 (sharp), 1/4.3 (strong/sharp, *arrow*), and 1/4.0Å^{-1} (diffuse). NOGS was then heated to 47°C, a temperature just beyond the endothermic transition observed in DSC experiments (see Fig. 5). The x-ray diffraction pattern in Fig. 6 *B* is dominated by form II of NOGS. The low-angle region shows lamellar reflections (h = 1–10), d = 69.9Å. The wide-angle region shows reflections at 1/5.5 (weak), 1/5.0 (sharp), 1/4.6 (diffuse, *arrow*), 1/4.4 (strong/sharp, *arrow*), 1/4.2 (sharp), and 1/3.9Å (diffuse). Clearly, forms I and II of NOGS are structurally different. After heating to 59°C, the x-ray diffraction pattern shown in Fig. 6 *C* is observed. The bilayer periodicity is reduced to d = 52.0Å, and the single diffuse reflection in the wide-angle region at 1/4.6Å^{-1} (*arrow*) is a characteristic of a melted-chain L_α bilayer phase.

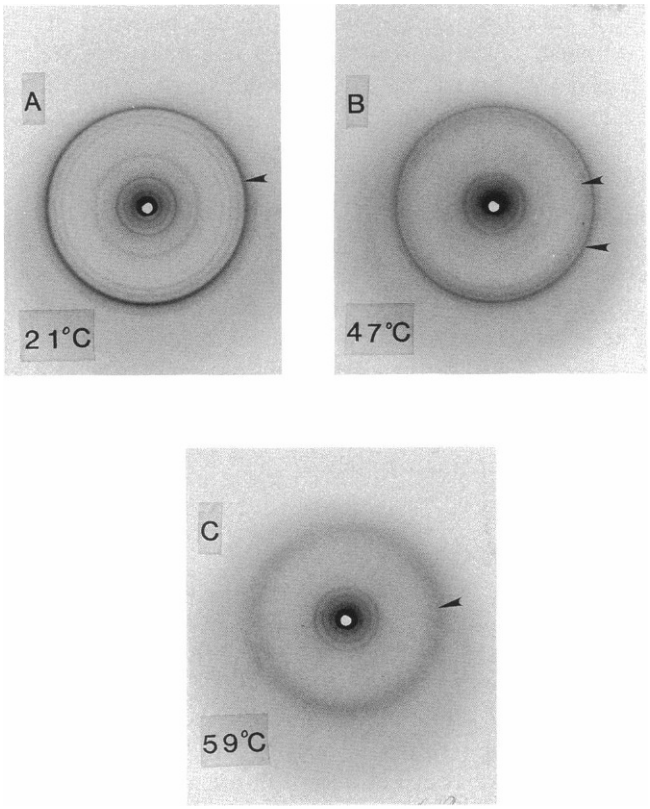

FIGURE 6 X-ray diffraction patterns of hydrated NOGS at (*A*) 21°C, (*B*) 47°C, and (*C*) 59°C.

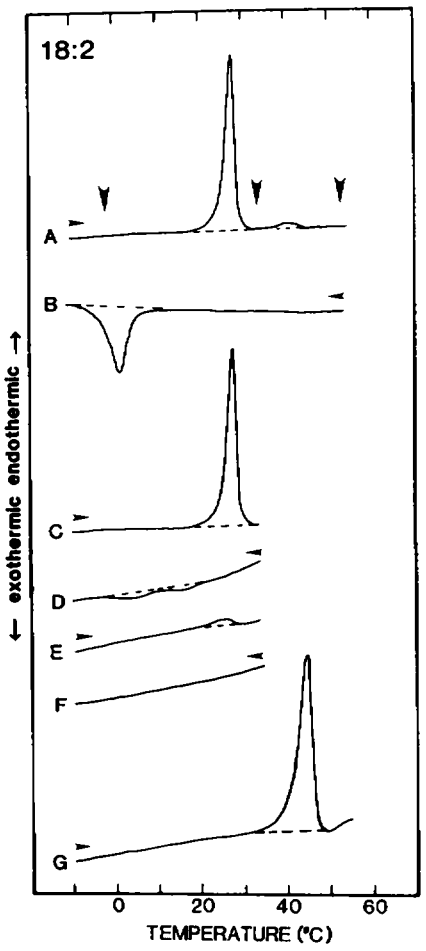

FIGURE 7 DSC scans of hydrated (70 wt % H_2O) NLnGS recorded at heating and cooling rates of 5°C/min. (*A*) Heating scan; (*B*) cooling scan; (*C*) heating scan to 32°C; (*D*) subsequent cooling scan after incubation at 32°C for 21.5 h; (*E*) immediate heating scan to 32°C; (*F*) subsequent cooling scan after incubation at 32°C for 30 min; (*G*) heating scan. (*Horizontal arrows*) Direction of heating/cooling scans. (*Vertical arrows*) Temperatures at which x-ray diffraction patterns were recorded.

NLnGS

The calorimetric behavior of hydrated (70 wt% H_2O) NLnGS (18:2) is depicted in Fig. 7. On heating at 5°C/min hydrated NLnGS gives two endothermic transitions in the temperature range from −10°C to 55°C. As indicated in Fig. 7 *A*, the first transition occurs at 28°C (ΔH = 8.0 kcal/mol NLnGS), whereas the second transition is broad with a peak maximum ~42°C ($\Delta H \simeq 0.4$ kcal/mol NLnGS). Upon cooling (Fig. 7 *B*), a single exothermic transition is observed at 2.1°C ($\Delta H = -6.5$ kcal/mol NLnGS). This large hysteresis effect on cooling is similar to that observed for hydrated NSGS and NOGS (see Figs. 1 and 5). The broad, endothermic transition observed at 42.0°C on heating was indicative of complex behavior, perhaps similar to that observed for hydrated NOGS. Thus, the sample was heated to 32°C (Fig. 7 *C*) and incubated for 21.5 h. Upon cooling the exothermic transition usually observed (cf. Fig. 7, *B* and *D*) has become greatly reduced in enthalpy ($\Delta H = -0.3$ kcal/mol) and more complex. Subsequent heating (Fig. 7 *E*) demonstrates the corresponding reduction in the original endotherm ($T_m \simeq 25$°C, $\Delta H = 0.3$ kcal/mol). After incubation (30 min) at 32°C, the cooling run (Fig. 7 *F*) shows no exothermic transitions. The subsequent heating scan (Fig. 7 *G*) shows no transitions in the temperature range from −10°C to 30°C. However, the original small transition at 42°C (Fig. 7 *A*) has become a high enthalpy (ΔH = 9.3 kcal/mol NLnGS), sharp transition at 44°C (Fig. 7 *G*). Cooling from a temperature greater than 44°C subsequently produces the heating and cooling behavior shown in Fig. 7, *A* and *B*, indicating formation of the original low-temperature phase (T_m = 28°C).

Thus, similar to NOGS, hydrated NLnGS exhibits two low-temperature phases. One form (form I) is produced upon cooling NLnGS from $T > 44$°C or upon immediate cooling from 32°C. This phase appears to be stable over

the temperature range from −10°C to 28°C, and undergoes an endothermic chain melting transition at 28°C. Incubation at 32–40°C induces the formation of a new phase (form II). This higher melting phase is stable over the temperature range from −10°C to 44°C, and undergoes an endothermic transition T_m at 44.0°C.

To define the structural changes occurring in hydrated NLnGS, x-ray diffraction patterns were recorded at different temperatures. The vertical arrows in Fig. 7 *A* correspond to temperatures at which the x-ray diffraction patterns shown in Fig. 8 were recorded. The diffraction pattern in Fig. 8 *A* was recorded after the sample was heated to 55°C, and immediately cooled slowly (~2.5°C/min) to 0°C (form I). The low-angle region shows lamellar reflections (h = 1–7) corresponding to a bilayer periodicity d = 55.2Å. The wide-angle region shows four reflections at 1/5.5 (weak), 1/5.0 (weak), 1/4.7 (weak), and 1/4.3Å^{-1} (strong, *arrow*) with possibly a weaker, diffuse reflection at 1/3.9Å^{-1}. Upon heating hydrated NLnGS to 34°C, the diffraction pattern shown in Fig. 8 *B* is obtained. The low-angle region shows a series of lamellar reflections (h = 1–10), d = 68.4Å. The third-order reflection is complicated by the presence of an additional reflection which indexes to a bilayer periodicity of d = 51.5Å (see below). The wide-angle region shows seven reflections. The reflections at 1/5.4 (weak), 1/5.0 (weak), 1/4.5 (weak), 1/4.3 (strong, *arrow*), 1/4.1 (weak), and 1/3.9Å^{-1} (diffuse) are associated with the high melting phase (form II), while the diffuse reflection observed at 1/4.6Å^{-1} is probably related to a liquid crystalline phase (see below). Further heating to 55°C produces the x-ray diffraction pattern shown in Fig. 8 *C*. The low angle region shows lamellar reflections (h = 1–4), d = 51.8Å, with a single diffuse reflection in the wide-angle region at 1/4.6Å^{-1} (*arrow*). These reflections identify a liquid crystalline L_α bilayer phase in which the hydrocarbon chains are melted.

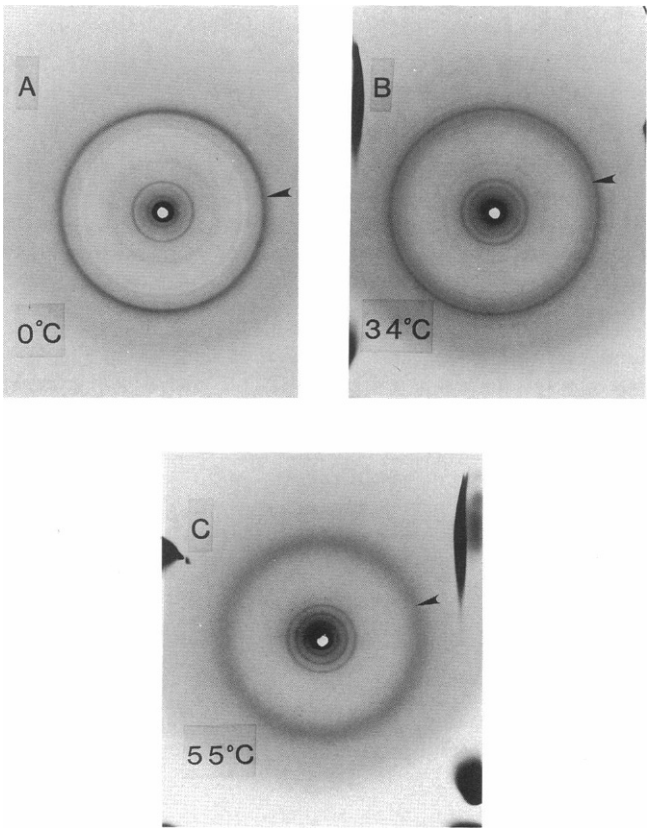

FIGURE 8 X-ray diffraction patterns of hydrated NLnGS at (*A*) 0°C; (*B*) 34°C, and (*C*) 55°C.

DISCUSSION

A summary of the structural changes occurring when hydrated NSGS, NOGS, and NLnGS are heated and cooled is shown in Fig. 9. When NSGS (18:0) is cooled from the liquid crystalline L_α phase two structural scenarios are possible (see Fig. 9, *top*). If NSGS is cooled very rapidly it converts at exotherm I into a metastable phase at ~50°C (see Figs. 1 and 2); the kinetically slow exotherm II prevents conversion of this phase into the stable phase at fast cooling rates. Thus, at low temperatures (20°C) the metastable phase predominates. X-ray diffraction indicates that this metastable phase is highly ordered (crystalline chain packing) and is similar in chain packing, at least, to the anhydrous, crystalline form of NSGS (Fig. 4). Upon heating this phase in the presence of excess water, an exothermic conversion of the metastable phase to the thermodynamically stable phase is observed over the range 40–60°C. The stable phase has been shown to be a bilayer structure also with crystalline chain packing (Fig. 3 *B*), and is stable over the temperature range of 5–80°C (Fig. 1). It is this phase which undergoes the high temperature (85°C), high enthalpy (18.0 kcal/mol) chain melting transition to the liquid crystalline phase.

Alternatively, slower cooling from the L_α phase leads to an exothermic conversion to the metastable phase followed by conversion of this phase (exotherm II) to the stable crystalline phase (Fig. 2). Hence, the slower cooling rate allows time for the process associated with exotherm II to occur. X-ray diffraction patterns collected after cooling at 2.5°C/min are identical to that of the stable phase shown in Fig. 3 *B* (data not shown). On heating, the stable phase shows no thermal transitions until the endothermic hydrocarbon chain melting at 85°C. Intermediate cooling rates lead to the coexistence of both phases at low temperatures.

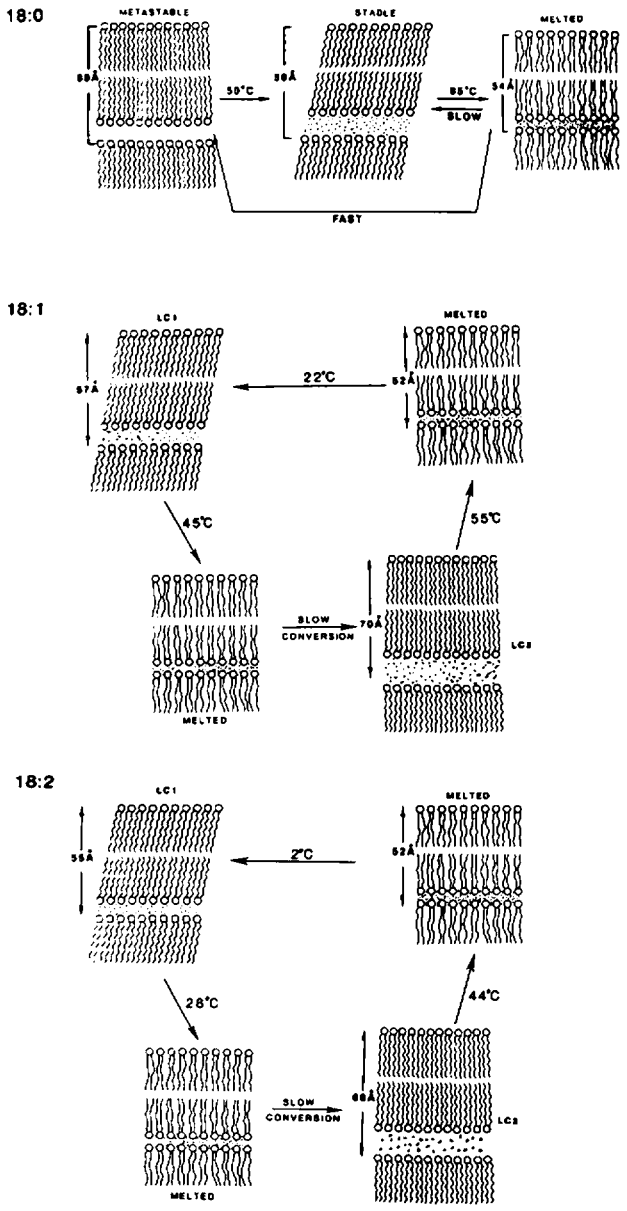

FIGURE 9 Summary of structural changes exhibited by NSGS (*top*), NOGS (*middle*), and NLnGS (*bottom*). The phases with crystalline chain packing modes are represented using ~~~ chains, whereas the melted chains are shown as ~~~. The evidence for chain tilt in the LC1 phases and lack of chain tilt in the LC2 phases is indirect and based only on the differences in bilayer periodicity. More extensive hydration studies or studies on oriented bilayers will be needed to characterize fully the chain tilt in the different phases.

The large number of reflections in the wide angle region for the stable phase, as well as the high enthalpy associated with its melting, indicates a highly ordered phase with respect to both interchain interactions and intra- and intermolecular interactions at the polar surface. The galactose in the headgroup contains hydroxyl groups capable of establishing a hydrogen bonding matrix, and the amide and hydroxyl groups at the interfacial region can also act as either donors or acceptors in the formation of an extensive hydrogen bonding network. Studies by Pascher and Sundell (1977) support the existence of an extensive hydrogen bonding matrix for these fully saturated cerebrosides. Since the metastable phase may be related to the anhydrous, crystalline form of NSGS, it seems likely that the rehydration, which occurs when the metastable phase converts to the stable phase, triggers a reordering of the hydrocarbon chains (see also Ruocco et al., 1981 and below). The metastable phase has a bilayer periodicity of d = 59.6Å, while the more hydrated stable phase has a periodicity of d = 58.4Å. Since the bilayer periodicity decreases on forming the stable phase, in spite of the rehydration, a tilting of the hydrocarbon chains is expected in the stable phase (see Fig. 9, *top*).

The behavior of hydrated NOGS (18:1) is summarized in Fig. 9, middle. The calorimetric and x-ray diffraction experiments show that the complexity associated with hydrated NOGS involves interconversions between two "stable" low-temperature phases. Upon cooling NOGS from $T > 55$°C (or $T > 45$°C when no incubations are performed), an exothermic transition centered at 22°C is observed. This transition represents the conversion of NOGS from a melted-chain, liquid crystalline bilayer phase to a low-temperature phase (form I). From the x-ray diffraction pattern (Fig. 6 *A*), the large number of reflections observed in the low angle region (h = 1–9) d = 56.5Å, indicates the presence of a highly ordered, stacked bilayer phase and the multiple wide-angle reflections show that the hydrocarbon chains have adopted one of the specific crystalline chain-packing arrangements defined by either a simple or complex subcell (Abrahamsson et al., 1978; Shipley, 1986; Ruocco and Shipley, 1982a,b). This phase will be referred to as the LC1 phase (instead of form I). Heating the LC1 phase produces no transition over the temperature range 0–40°C, with further heating leading to an endothermic transition with T_m = 44.8°C (ΔH = 11.5 kcal/mol NOGS). This probably represents the conversion of NOGS from the LC1 phase to a melted-chain, L_α phase. Some x-ray diffraction patterns (data not shown) recorded at a temperature $45 < T < 55$°C indicate the coexistence of the L_α phase (one reflection in the low-angle region, d = 52Å, and a diffuse reflection in the wide-angle region at $\sim -1/4.6\text{Å}^{-1}$) with the phase described below. However, an incubation protocol in which hydrated NOGS is kept at 49°C for 24 h, cooled, and reincubated for another 70 min at the same temperature, produces calorimetrically a single high melting phase at 55°C (ΔH = 12.0 kcal/mol). Alternatively, several incubations of shorter duration at 49°C will also produce this high melting phase. By x-ray diffraction

(Fig. 6 *B*), the new phase has an increased bilayer periodicity (d = 69.9Å) and the large number of wide-angle reflections again indicate a bilayer phase in which the hydrocarbon chains are packed into a crystalline arrangement. It appears that the L_α phase is metastable at this temperature and converts slowly to the stable, high melting phase. This new, high melting phase, previously designated form II, will be referred to as the LC2 phase. The difference in bilayer periodicity (56.5 vs. 69.9Å), as well as the difference in the wide-angle reflections clearly show that LC1 and LC2 are two distinct, but both crystalline, bilayer phases.

Upon complete formation of the LC2 phase, the absence of transitions in the temperature range 0–50°C show that it is now the stable phase over this temperature range. Interestingly, after incubations at 47°C for intermediate times (data not shown), the exotherm observed originally on cooling at 22°C (see Fig. 5 *B*) occurs at 28°C. This increase in the temperature of the exothermic transition is probably caused by the presence of the LC2 phase formed during the incubation, which affects the recrystallization of the LC1 phase from the melted-chain, L_α phase. Heating the pure LC2 phase produces an endothermic transition at 55°C. The phase formed upon melting the LC2 phase has been clearly identified as a liquid crystalline, L_α bilayer phase. Liquid crystalline phases have been observed in phospholipids (Ruocco and Shipley, 1982a,b), glycolipids (Shipley et al., 1973), and other glycosphingolipids (Ruocco et al., 1981). Cooling from this phase leads to the exothermic "crystallization" of the LC1 phase.

A summary of the thermotropic properties of hydrated NLnGS (18:2) is presented in Fig. 9 (*bottom*). Cooling NLnGS from the L_α, bilayer phase (either at $28 < T < 40$°C without incubations, or $T > 44$°C) leads to an exothermic recrystallization of the hydrocarbon chains (ΔH = −6.5 kcal/mol NLnGS) at ~2°C. X-ray diffraction indicates that this phase is lamellar (d = 55.2Å) and the hydrocarbon chains have adopted one of the specific crystalline chain-packing arrangements. The diffraction pattern is essentially identical to that of the low melting phase of NOGS (cf. Figs. 6 *A* and 8 *A*); this phase will be referred to as the LC1 phase. This phase is stable over the temperature range −10–28°C, and undergoes endothermic chain melting at 28°C to a liquid crystalline phase, which slowly converts to a stable, higher melting phase. Thus, x-ray diffraction at 33°C indicates the predominance of a phase which has a bilayer periodicity of d = 68.4Å, and again a crystalline arrangement of the hydrocarbon chains; differences in the positions of several of the wide-angle reflections of this high melting phase when compared to the LC1 phase indicate that the chain packing interactions in the two phases differ (see Fig. 8, *A* and *B*). Since the high melting phase of NLnGS is crystalline and virtually identical to that of NOGS (cf. Figs. 6 *B* and 8 *B*), it will be referred to as the LC2 phase. The low angle reflection, d = 51.5Å, in addition to a diffuse reflection at 1/4.6Å indicates the presence of some unconverted L_α phase.

For the LC2 phase, the absence of transitions in the range of −10–40°C demonstrates its thermodynamic stability (see Fig. 7, *F* and *G*). Further heating leads to an endothermic transition at 44°C in which the crystalline hydrocarbon chains melt (ΔH = 9.3 kcal/mol NLnGS). X-ray diffraction at $T > 50$°C indicates that NLnGS forms a melted chain, L_α bilayer phase, bilayer periodicity d = 51.8Å. Cooling from this L_α phase produces the LC1 phase. To date, no way has been found to go directly from an L_α phase at $T > 44$°C to the LC2 phase on cooling.

Shorter-term incubations of either NOGS or NLnGS lead to the coexistence of both phases at low temperatures. Calorimetric experiments in which either NOGS or NLnGS were incubated for 4–5 h at a temperature intermediate between the melting temperatures of their respective LC1 and LC2 phases, then cooled and reheated, indicated the presence of both the LC1 and LC2 phases (data not shown). Similarly, for both NOGS and NLnGS, x-ray diffraction patterns recorded at low temperature after the 4–5 h incubation shows two sets of low-angle reflections which index to lamellar periods characteristic of both their respective LC1 and LC2 phases, as well as reflections in the wide-angle region associated with both the LC1 and LC2 phases (data not shown).

In previous studies concerning the structure and thermotropic properties of hydrated and anhydrous NPGS (Ruocco et al., 1981), it was shown that upon heating equilibrated, hydrated NPGS, a high-temperature (82°C) and high-enthalpy (17.5 kcal/mol NPGS) transition from a stable crystalline phase to a melted-chain bilayer phase occurred. Slowly cooling hydrated NPGS from the L_α phase led to the exothermic formation of a metastable phase at 62°C which then converted exothermically into the stable crystalline phase at 52°C. Rapidly cooling hydrated NPGS formed only the metastable phase at low temperatures (20°C). Incubation of this metastable phase at 20°C for many hours led to a time-dependent conversion to the stable crystalline phase. Thus, on cooling, a time-dependent process was recognized in forming the stable phase from the metastable phase. Heating the metastable phase from low temperatures led to an exothermic crystallization of the stable phase. In this case, x-ray diffraction demonstrated that the metastable phase was essentially identical to an anhydrous form of NPGS. Therefore, rapid cooling of hydrated NPGS led to a dehydration of NPGS (forming

the metastable phase) which then rehydrated and recrystallized in a time- and temperature-dependent event to form the stable phase.

Clearly NPGS and NSGS differing only in two methylene groups in the amide-linked hydrocarbon chain exhibit similar thermotropic behavior. The wide-angle diffraction patterns of the stable phases of NPGS (see Ruocco et al., 1981) and NSGS (see Fig. 3 *B*) are very similar, indicating structural homology. For NPGS d = 54.4Å (stable), while for NSGS d = 58.4Å (stable). In the stable phases, the bilayer periods differ by 4Å, in reasonable agreement with the predicted difference of 5Å assuming identical hydration, identical chain tilt, and no chain interdigitation. The same argument holds for the L_α phases, with a bilayer increase of ~3Å expected for the additional methylene groups on the NSGS, again assuming identical hydration and no chain interdigitation. Experimentally, the bilayer periodicities of the L_α phases of NPGS and NSGS differ by 2.7Å. Owing to different kinetics of rehydration, the metastable phases of NPGS and NSGS are more difficult to compare. However, for both NPGS and NSGS the wide-angle diffraction patterns are dominated by the strong ~1/4.4 and ~1/3.9Å^{-1} reflections. Therefore the metastable phase of NSGS is most likely a dehydrated phase, as was shown more clearly for NPGS (Ruocco et al., 1981).

The effect of increasing chain unsaturation in the amide-linked hydrocarbon chain, but keeping the chain length constant (C18), is a decrease in the chain-melting transition temperature as well as its associated enthalpy. Considering the LC1 phase, the addition of a single *cis* double bond (Δ9–10) in the hydrocarbon chain (NOGS) results in a 40°C decrease in T_m and a 6.5-kcal/mol decrease in its enthalpy. The *cis* double bond produces a kink in the hydrocarbon chain which affects the chain packing arrangements. The decrease in chain packing order leads to a reduction in the energy necessary for disruption of these stabilizing interactions and thus the lower T_m and ΔH observed. For NLnGS with two *cis* double bonds (Δ9–10, Δ12–13), a further reduction in main chain melting by 17°C (from 45°C in NOGS to 28°C in NLnGS) and a corresponding enthalpy decrease of 3.1 kcal/mol (from 11.5 kcal/mol in NOGS to 8.4 kcal/mol in NLnGS) is observed. These comparisons are complicated by the presence of a high-melting crystalline phase (LC2) for each of the unsaturated galactosyl cerebrosides. If this phase is compared to NSGS, then the decrease in T_m in adding a single *cis* double bond is 30°C, while the second *cis* double bond leads to a further 11°C decrease.

The effect of increasing unsaturation in the galactosyl cerebrosides is similar to that observed in phospholipids. For C_{18}-phosphatidylcholines the introduction of the first *cis* double bond (Δ9–10) in the acyl chain (at the *sn*-2 position) resulted in a 50°C decrease in the chain-melting transition ($P_{\beta'} \rightarrow L_\alpha$), while an additional *cis* double bond (Δ12–13) led to a further decrease in T_m by 22°C (Coolbear et al., 1983; see also Stubbs et al., 1981). This reduction in transition temperature is similar to that observed for the unsaturated-chain galactosyl cerebrosides, described above. Thus, the overall conclusion is that the introduction of unsaturated chains into the bilayer drastically affects the chain–chain interactions leading to a reduction in the chain melting transition temperature and enthalpy, even though the interactions at the headgroup regions of the PC and cerebroside systems differ markedly.

We thank Drs E. Oldfield and R. Skarjune (University of Illinois) for supplying the cerebrosides used in this study. We thank David Jackson for technical help, Dr. D. Atkinson for advice, and Irene Miller for help in preparing the manuscript.

This research was supported by research grant HL-26335 and training grants HL-07429 and HL-07224 from the National Institutes of Health.

Received for publication 25 July 1988 and in final form 24 October 1988.

REFERENCES

Abrahamsson, S., I. Pascher, K. Larsson, and K.-A. Karlsson. 1972. Molecular arrangements in glycosphingolipids. *Chem. Phys. Lipids.* 8:152–179.

Abrahamsson, S., B. Dahlen, H. Lofgren, and I. Pascher. 1978. Lateral packing of hydrocarbon chains. *Prog. Chem. Fats Other Lipids.* 16:125–143.

Bunow, M. R. 1979. Two gel states of cerebrosides: calorimetric and Raman spectroscopic evidence. *Biochim. Biophys. Acta.* 574:542–546.

Bunow, M. R., and I. W. Levin. 1980. Molecular conformations of cerebrosides in bilayers determined by Raman spectroscopy. *Biophys. J.* 32:1007–1022.

Clowes, A. W., R. J. Cherry, and D. Chapman. 1971. Physical properties of lecithin-cerebroside bilayers. *Biochim. Biophys. Acta.* 249:301–317.

Coolbear, K. P., C. B. Berde, and K. M. W. Keough. 1983. Gel to liquid-crystalline phase transitions of aqueous dispersions of polyunsaturated mixed-acid phosphatidylcholines. *Biochemistry.* 22:1466–1473.

Curatolo, W. 1982. Thermal behavior of fractionated and unfractionated bovine brain cerebrosides. *Biochemistry.* 21:1761–1764.

Curatolo, W., and F. B. Jungalwala. 1985. Phase behavior of galactocerebrosides from bovine brain. *Biochemistry.* 24:6608–6613.

Fernandez-Bermudez, S., J. Loboda-Cackovic, H. Cackovic, and R. Hosemann. 1977. Structure of cerebrosides. I. Phrenosine at 23°C and 66°C. *Z. Naturforsch.* 32C:362–374.

Freire, E., D. Bach, M. Correa-Freire, I. Miller, and Y. Barenholz. 1980. Calorimetric investigation of the complex phase behavior of glucocerebroside dispersions. *Biochemistry*. 19:3662–3665.

Gounaris, K., D. A. Mannock, A. Sen, A. P. R. Brain, W. P. Williams, and P. J. Quinn. 1983. Polyunsaturated fatty acyl residues of galactolipids are involved in the control of bilayer/non-bilayer lipid transitions in higher plant chloroplasts. *Biochim. Biophys. Acta*. 732:229–242.

Hosemann, R., J. Loboda-Cackovik, H. Cackovic, S. Fernandez-Bermudez, and F. J. Balta-Calleja. 1979. Structure of cerebrosides. II. Small angle x-ray diffraction study of cerasine. *Z. Naturforsch.* 34C:1121–1124.

Huang, T. H., R. P. Skarjune, R. J. Wittebort, R. G. Griffin, and E. Oldfield. 1980. Restricted rotational isomerization in polymethylene chains. *J. Am. Chem. Soc.* 102:7377–7379.

Lee, D. C., I. R. Miller, and D. Chapman. 1986. An infrared spectroscopic study of metastable and stable forms of hydrated cerebroside bilayers. *Biochim. Biophys. Acta*. 859:266–270.

Linington, C., and M. G. Rumsby. 1978. On the accessibility and localisation of cerebrosides in central nervous system myelin. Adv. Exp. Med. Biol. 100:263–273.

Linington, C., and M. G. Rumsby. 1981. Galactosyl ceramides of the myelin sheath: thermal studies. *Neurochem. Int.* 3:211–218.

Maggio, B., F. A. Cumar, and R. Caputto. 1978a. Surface behaviour of gangliosides and related glycosphingolipids. *Biochem. J.* 171:559–565.

Maggio, B., F. A. Cumar, and R. Caputto. 1978b. Interactions of gangliosides with phospholipids and glycosphingolipids in mixed monolayers. *Biochem. J.* 175:1113–1118.

Maggio, B., F. A. Cumar, and R. Caputto. 1981. Molecular behaviour of glycosphingolipids in interfaces: possible participation in some properties of nerve membranes. *Biochim. Biophys. Acta*. 650:69–87.

Mannock, D. A., A. P. R. Brain, and W. P. Williams. 1985. The phase behavior of 1,2-diacyl-3-monogalactosyl-*sn*-glycerol derivatives. *Biochim. Biophys. Acta*. 817:289–298.

Mansourian, A. R., and P. J. Quinn. 1986. Phase properties of binary mixtures of monogalactosyldiacylglycerols differing in hydrocarbon chain substituents dispersed in aqueous systems. *Biochim. Biophys. Acta*. 855:169–178.

Pascher, I., and S. Sundell. 1977. Molecular arrangements in sphingolipids: the crystal structure of cerebroside. *Chem. Phys. Lipids*. 20:175–191.

Radin, N. S. 1972. Labeled galactosyl ceramide and lactosyl ceramide. *Methods Enzymol.* 28:300–306.

Radin, N. S. 1974. Preparation of psychosines (1-O-hexosylsphingosine) from cerebrosides. *Lipids*. 9:358–360.

Radin, N. S. 1976. Preparative isolation of cerebrosides (galactosyl and glucosyl ceramide). *J. Lipid Res.* 17:290–293.

Reed, R. A., and G. G. Shipley. 1987. Structure and metastability of *N*-lignocerylgalactosylsphingosine (cerebroside) bilayers. *Biochim. Biophys. Acta*. 896:153–164.

Reiss-Husson, F. 1967. Structure des phases liquide—cristallines de différents phospholipides, monoglycérides, sphingolipides, anhydres ou en présence d'eau. *J. Mol. Biol.* 25:363–382.

Rumsby, M. G. 1978. Organization and structure in central-nerve myelin. *Biochem. Soc. Trans.* 6:448–462.

Ruocco, M. J., D. Atkinson, D. M. Small, R. P. Skarjune, E. Oldfield, and G. G. Shipley. 1981. X-ray diffraction and calorimetric study of anhydrous and hydrated *N*-palmitoylgalactosylsphingosine (cerebroside). *Biochemistry*. 20:5957–5966.

Ruocco, M. J., and G. G. Shipley. 1982a. Characterization of the sub-transition of hydrated dipalmitoylphosphatidylcholine bilayers: x-ray diffraction study. *Biochim. Biophys. Acta*. 684:59–66.

Ruocco, M. J., and G. G. Shipley. 1982b. Characterization of the sub-transition of hydrated dipalmitoylphosphatidylcholine bilayers: kinetic, hydration and structural study. *Biochim. Biophys. Acta*. 691:309–320.

Sen, A., W. P. Williams, and P. J. Quinn. 1981. The structure and thermotropic properties of pure 1,2-diacylgalactosylglycerols in aqueous systems. *Biochim. Biophys. Acta*. 663:380–389.

Shipley, G. G., J. P. Green, and B. W. Nichols. 1973. The phase behavior of monogalactosyl, digalactosyl, and sulphoquinovosyl diglycerides. *Biochim. Biophys. Acta*. 311:531–544.

Shipley, G. G. 1986. X-ray crystallographic studies of aliphatic lipids. *In* Handbook of Lipid Research. Vol. 4. D. M. Small, editor. Plenum Press, New York. 97–147.

Skarjune, R., and E. Oldfield. 1979. Physical studies of cell surface and cell membrane structure: deuterium nuclear magnetic resonance investigation of deuterium-labelled *N*-hexadecanoylgalactosylceramides (cerebrosides). *Biochim. Biophys. Acta*. 556:208–218.

Skarjune, R., and E. Oldfield. 1982. Physical studies of cell surfaces and cell membrane structure: deuterium nuclear magnetic resonance studies of *N*-palmitoylglucosylceramide (cerebroside) head group structure. *Biochemistry*. 21:3154–3160.

Stubbs, C. D., T. Kouyama, K. Kinosita, Jr., and A. Ikegami. 1981. Effect of double bonds on the dynamic properties of the hydrocarbon region of lecithin bilayers. *Biochemistry*. 20:4257–4262.